Hot-Electron Transfer from Semiconductor Nanocrystals

William A. Tisdale, *et al.*

Science **328**, 1543 (2010);
DOI: 10.1126/science.1185509

Microgravity enables us to venture into the regime of unprecedented long time evolution of the BEC up to 1 s (Fig. 4, B and D) with our setup. Our measurements reveal the above-mentioned suppression of the expansion in the x direction. Although our theory (black solid curves) predicts a linear growth, we observe a saturation. In addition, the observed widths in the z direction are larger than expected.

The origin of both deviations can be traced back to the fact that, during the expansion phase, the atoms are in the $F = 2$, $m_F = 2$ hyperfine state. Because of the long expansion times, these deviations represent a sensitive probe of tiny magnetic field gradients and curvatures. By including magnetic field curvatures on the order of a few microtesla per square millimeter in our simulation (black dotted curves), we are able to provide a qualitative explanation of the observed half widths. A coherent transfer of the BEC into the magnetically insensitive hyperfine state $F = 2$, $m_F = 0$ would avoid the influence of parasitic effects, and the implementation of this transfer is currently under way.

We anticipate a multitude of new research directions for ultracold, dilute quantum gases in free fall. A spin-off from our experiment is the possibility of preparing an extremely dilute wave packet at the lowest energy scales. This limit is difficult to reach in standard BEC experiments but is relevant for the observation of quantum reflection (*25*) or Anderson localization (*26*, *27*). Future atom interferometers in space will probe the boundary between GR and QM.

References and Notes

1. C. W. Misner, K. S. Thorne, J. A. Wheeler, *Gravitation* (Freeman, San Francisco, 1973).
2. E. A. Cornell, C. E. Wieman, *Rev. Mod. Phys.* **74**, 875 (2002).
3. W. Ketterle, *Rev. Mod. Phys.* **74**, 1131 (2002).
4. G. Stern *et al.*, *Eur. Phys. J. D* **53**, 353 (2009).
5. E. Arimondo, W. Ertmer, W. P. Schleich, E. M. Rasel, Eds., *Proceedings of the International School of Physics "Enrico Fermi" Course CLXVIII "Atom Optics and Space Physics"* (IOS Press, Bologna, Italy, 2009).
6. P. R. Berman, Ed., *Atom Interferometry* (Academic Press, San Diego, CA, 1997).
7. A. Peters, K. Y. Chung, S. Chu, *Nature* **400**, 849 (1999).
8. W. P. Schleich, M. O. Scully, in *New Trends in Atomic Physics, Proceedings of the Les Houches Summer School 1982, Session XXXVIII*, G. Grynberg, R. Stora, Eds. (North-Holland, Amsterdam, 1984), pp. 995–1124.
9. I. Ciufolini, E. C. Pavlis, *Nature* **431**, 958 (2004).
10. I. Ciufolini, *Nature* **449**, 41 (2007).
11. I. Ciufolini, J. A. Wheeler, *Gravitation and Inertia* (Princeton Univ. Press, Princeton, NJ, 1995).
12. S. Fray, C. Alvarez Diez, T. W. Hänsch, M. Weitz, *Phys. Rev. Lett.* **93**, 240404 (2004).
13. S. Dimopoulos, P. W. Graham, J. M. Hogan, M. A. Kasevich, *Phys. Rev. Lett.* **98**, 111102 (2007).
14. S. Dimopoulos, P. W. Graham, J. M. Hogan, M. A. Kasevich, S. Rajendran, *Phys. Rev. D Part. Fields Gravit. Cosmol.* **78**, 122002 (2008).
15. A. E. Leanhardt *et al.*, *Science* **301**, 1513 (2003).
16. A. Vogel *et al.*, *Appl. Phys. B* **84**, 663 (2006).
17. W. Hänsel, P. Hommelhoff, T. W. Hänsch, J. Reichel, *Nature* **413**, 498 (2001).
18. R. Folman, P. Krüger, J. Schmiedmayer, J. Denschlag, C. Henkel, *Adv. At. Mol. Opt. Phys.* **48**, 263 (2002).
19. J. Fortágh, C. Zimmermann, *Rev. Mod. Phys.* **79**, 235 (2007).
20. Y. Kagan, E. L. Surkov, G. V. Shlyapnikov, *Phys. Rev. A* **54**, R1753 (1996).
21. Y. Castin, R. Dum, *Phys. Rev. Lett.* **77**, 5315 (1996).
22. P. Storey, M. Olshanii, *Phys. Rev. A* **62**, 033604 (2000).
23. Materials and methods are available as supporting material on *Science* Online.
24. G. Nandi, R. Walser, E. Kajari, W. P. Schleich, *Phys. Rev. A* **76**, 063617 (2007).
25. T. A. Pasquini *et al.*, *Phys. Rev. Lett.* **97**, 093201 (2006).
26. J. Billy *et al.*, *Nature* **453**, 891 (2008).
27. G. Roati *et al.*, *Nature* **453**, 895 (2008).

28. This project is supported by the German Space Agency Deutsches Zentrum für Luft- und Raumfahrt (DLR) with funds provided by the Federal Ministry of Economics and Technology (BMWi) under grant number DLR 50 WM 0346. We thank the German Research Foundation for funding the Cluster of Excellence QUEST Centre for Quantum Engineering and Space-Time Research.

Supporting Online Material

www.sciencemag.org/cgi/content/full/328/5985/1540/DC1
Materials and Methods
References

5 March 2010; accepted 10 May 2010
10.1126/science.1189164

Hot-Electron Transfer from Semiconductor Nanocrystals

William A. Tisdale,[1] Kenrick J. Williams,[2,3]* Brooke A. Timp,[2] David J. Norris,[1]† Eray S. Aydil,[1]† X.-Y. Zhu[2,3]*†

In typical semiconductor solar cells, photons with energies above the semiconductor bandgap generate hot charge carriers that quickly cool before all of their energy can be captured, a process that limits device efficiency. Although fabricating the semiconductor in a nanocrystalline morphology can slow this cooling, the transfer of hot carriers to electron and hole acceptors has not yet been thoroughly demonstrated. We used time-resolved optical second harmonic generation to observe hot-electron transfer from colloidal lead selenide (PbSe) nanocrystals to a titanium dioxide (TiO_2) electron acceptor. With appropriate chemical treatment of the nanocrystal surface, this transfer occurred much faster than expected. Moreover, the electric field resulting from sub–50-femtosecond charge separation across the PbSe-TiO_2 interface excited coherent vibrations of the TiO_2 surface atoms, whose motions could be followed in real time.

The maximum theoretical efficiency of a standard silicon solar cell in use today is limited to ~31%, in part by the loss of any photon energy that exceeds the semiconductor bandgap (*1*). Absorption of high-energy photons creates hot electrons and holes that cool quickly (within ~1 ps) to the band edges by sequential emission of phonons. There the carriers remain for hundreds of picoseconds or longer before slower processes such as radiative or nonradiative recombination occur. The goal of standard solar cells is to extract these band-edge electrons and holes to produce electrical current. However, because of the initial cooling process, a substantial amount of solar energy has already been irreversibly lost. If instead, all of the energy of the hot carriers could be captured, solar-to-electric power conversion efficiencies could be increased, theoretically to as high as 66% (*2*). We can envision the realization of such a hot carrier solar cell in a semiconductor device where scattering among photoexcited electrons and reabsorption of additional photons in the conduction band is faster than hot-electron cooling, resulting in a quasi-equilibrium characterized by an electron temperature much higher than the lattice temperature. This is coupled with equally fast hot-electron transfer to an electron conductor in a narrow energy window (to minimize additional energy loss in the latter). The same argument applies to the holes.

A potential route to the above hot carrier solar cell is to use semiconductor nanocrystals, or quantum dots (*3*). In these materials, the quasi-continuous conduction and valence energy bands of the bulk semiconductor become discretized owing to confinement of the charge carriers. Consequently, the energy spacing between the electronic levels can be much larger than the highest phonon frequency of the lattice, creating a "phonon bottleneck" in which hot-carrier relaxation is only possible via slower multiphonon emission (*4*). For example, hot-electron lifetimes as long as ~1 ns have been

[1]Department of Chemical Engineering and Materials Science, University of Minnesota, Minneapolis, MN 55455, USA. [2]Department of Chemistry, University of Minnesota, Minneapolis, MN 55455, USA. [3]Department of Chemistry and Biochemistry, University of Texas, Austin, TX 78712, USA.

*Present address: Department of Chemistry and Biochemistry, University of Texas, Austin, TX 78712, USA.
†To whom correspondence should be addressed: zhu@cm.utexas.edu (X.-Y.Z.), dnorris@umn.edu (D.J.N.), aydil@umn.edu (E.S.A.)

observed in quantum dots grown by molecular beam epitaxy (*5*). Even in colloidal quantum dots, which are coated with surfactant molecules that provide additional high-frequency vibrations for carrier relaxation, long lifetimes have been demonstrated through careful design of core-shell structures and control of interfaces (*6*). Such slowing of electron relaxation in core-shell quantum dots has recently been shown to allow the tunneling of hot electrons through the shells to surface trap states (*7*). Because of their ability to slow electronic relaxation, quantum dots can in principle enable extraction of hot carriers (to electron or hole conductors) before they cool to the band edges, leading to more efficient solar cells (*8*). However, hot-carrier transfer from nanocrystals to an electron or hole conductor has not yet been observed. Here, we show that electron transfer from the higher excited states of a colloidal semiconductor nanocrystal (PbSe) to a common electron acceptor (TiO_2) is indeed possible and, with appropriate chemical treatment of the nanocrystal surface, occurs on an ultrafast time scale (<50 fs).

Although heterogeneous electron transfer from molecular chromophores to metal-oxide semiconductors has been probed with femtosecond time-resolved absorption (*9*), extending this approach to quantum dots has proved challenging. Differentiating between transient spectroscopic signatures of the photoexcited quantum dot, the reduced TiO_2 substrate, and the trap states is difficult (*10*). Further, to generate adequate signal, porous samples with large surface area but poorly defined interfaces are used. Consequently, reported time scales have spanned from picoseconds to microseconds (*10*–*13*).

Optical second harmonic generation (SHG) (*14*) is a much better technique for studying quantum-dot–to–semiconductor electron transfer because it offers femtosecond time resolution with sufficient sensitivity for well-defined crystalline interfaces. In a centrosymmetric semiconductor such as rutile TiO_2, the second harmonic response originates only from the first few atomic layers near the surface (*15*). Thus, SHG should be extremely sensitive to changes in the local electronic environment resulting from interfacial electron transfer. Indeed, SHG has been used to probe ultrafast electron transfer at liquid-liquid interfaces (*16*). We show here that it can also be applied to semiconductor interfaces.

For fast electron transfer to occur, the nanocrystals should exhibit strong electronic coupling to the substrate. We chose colloidal PbSe quantum dots, as they are easy to prepare (*17*) and are better suited for electron transfer than other possible materials. In particular, PbSe has an extremely large exciton Bohr radius (46 nm) such that charge carriers in sub–10-nm diameter PbSe quantum dots are subject to strong quantum confinement effects (*18*), and their electronic wave functions will extend spatially well beyond the nanocrystal surface. This delocalization facilitates electron transfer if the nanocrystals are close to an electron accepting substrate. We chose rutile TiO_2 for this role because it not only is technologically relevant and available as a single crystal but also has a very large density of accepting states. Further, the (110) surface of rutile TiO_2 is one of the most studied metal oxide interfaces, and the surface nonlinear susceptibility tensor and the origins of the second harmonic response are known (*15*).

Each sample consisted of one or two monolayers of PbSe nanocrystals deposited on atomically flat single-crystalline (110) TiO_2 (Fig. 1, A and B). The films were chemically treated with either hydrazine or 1,2-ethanedithiol (EDT) (*19*) to respectively remove or substitute for the oleic acid present on the nanocrystal surface. Both treatments enhance electronic coupling to the TiO_2 substrate and within the film (*17*, *20*–*22*), but the bare surfaces produced by hydrazine result in stronger coupling (fig. S3). However, hydrazine can also leave many dangling bonds at the nanocrystal surface that can presumably act as scattering sites and accelerate electronic cooling within the quantum dot. In contrast, thiols such as EDT passivate the nanocrystal surface and slow hot-electron relaxation in colloidal nanocrystals (*6*).

We tested PbSe nanocrystals ranging in diameter from 3.3 to 6.7 nm. As with all strongly confined semiconductor nanocrystals, the energy of excited electron states in PbSe quantum dots increases with decreasing particle size. Thus, we first used ultraviolet photoelectron spectroscopy, in conjunction with optical absorption, to determine the energy of the lowest excited electronic state in our nanocrystals (*19*). We found that, regardless of particle size or chemical treatment, this state was always below the TiO_2 conduction band minimum (Fig. 1C). As a result, electron transfer from PbSe to TiO_2 should only be possible from hot electronic states of the quantum dot (*12*).

To study this electron transfer, we used 50-fs pulses of 810-nm (1.53-eV) light both to photoexcite (pump) the nanocrystals and detect (probe) the second harmonic response (*19*). The intensity of reflected second harmonic light at 405 nm ($I^{2\omega}$)

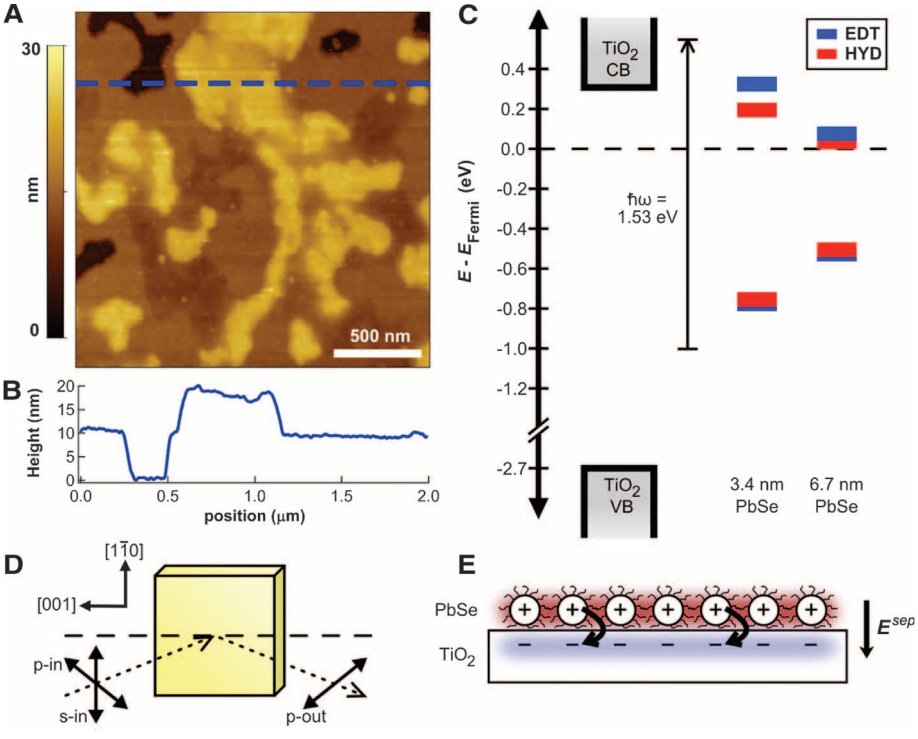

Fig. 1. (**A**) Atomic force micrograph showing the morphology of a ~1.5-monolayer film of 6.7-nm oleic acid–capped PbSe nanocrystals supported on atomically flat TiO_2. (**B**) Line height profile corresponding to the dashed blue line in (A). The height of a monolayer (~11 nm) is the diameter of a nanocrystal (~7 nm) plus the thickness of the passivating organic layer (~2 nm) both above and below. (**C**) Alignment of highest occupied and lowest unoccupied quantum dot energy levels relative to the TiO_2 conduction band edge after chemical treatment of the nanocrystal surface. Alignment is determined by ultraviolet photoelectron and near-infrared absorption spectroscopies and indicates that electron transfer from the lowest excited state of the quantum dot is not energetically possible. The vertical arrow depicts symmetric photoexcitation of the PbSe quantum dots with 810-nm light. Numerical values are available in table S1. VB, valence band; CB, conduction band; EDT, 1,2-ethanedithiol; HYD, hydrazine. (**D**) Illustration of the crystal orientation and optical polarization used for SHG in reflection from the rutile (110) surface. (**E**) Schematic representation of the interfacial electric field generated by separation of electrons and holes across the PbSe-TiO_2 interface. Red indicates positive charge density; blue, negative charge density.

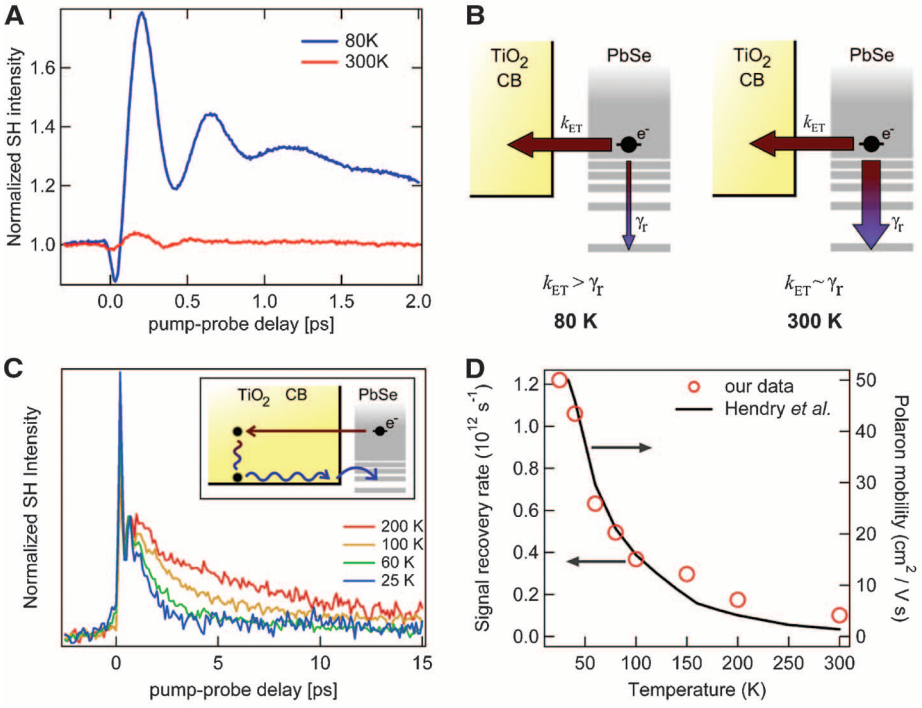

Fig. 2. (**A**) Time-resolved second harmonic response of the TiO_2 surface coated with 1.5 monolayers of hydrazine-treated 3.3-nm PbSe nanocrystals. The large rise in SHG intensity is indicative of efficient electron transfer from PbSe to TiO_2. (**B**) Illustration of the competing pathways of interfacial electron transfer and intra–quantum-dot relaxation. At higher temperatures, hot-electron relaxation (γ_r) becomes competitive with interfacial electron transfer (k_{ET}). (**C**) Temperature-dependent decay of the pump-induced SHG signal enhancement; the absolute intensity has been normalized for pump-induced change to better illustrate the temperature-dependent recovery rate. (Inset) Cartoon showing ballistic electron injection (straight arrow) followed by phonon scattering and polaronic transport back to the interface (wavy lines) and then transfer back to the nanocrystal (curved arrow). (**D**) Correlation of SHG signal recovery rate (red circles) with the temperature-dependent polaron mobility perpendicular to the *c* axis in TiO_2 measured previously (*29*) assuming a temperature-independent polaron effective mass (black line).

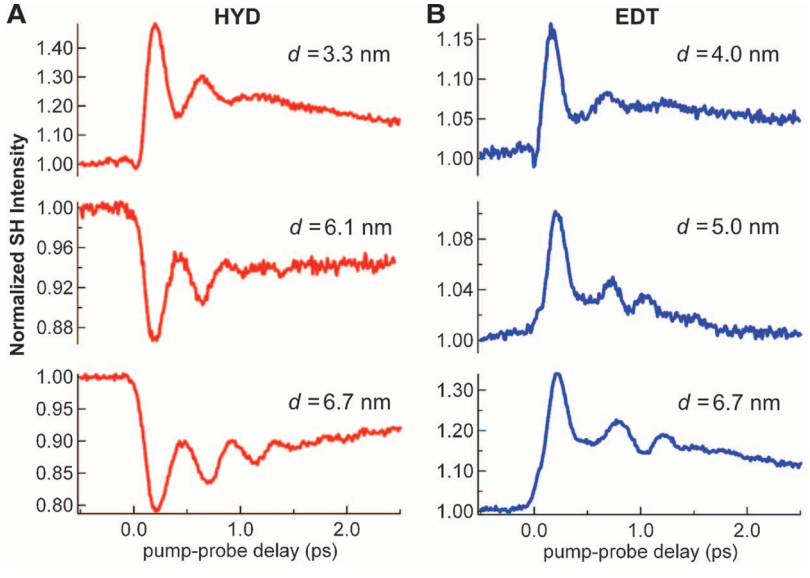

Fig. 3. Dependence of the time-resolved second harmonic response on nanocrystal size after treatment with (**A**) hydrazine (HYD) or (**B**) 1,2-ethanedithiol (EDT). The EDT-treated nanocrystals display efficient hot-electron transfer for all sizes studied, whereas substantial hot-electron transfer is only observed for smaller nanocrystals treated with hydrazine.

was recorded as a function of time delay between the pump and probe pulses. The polarization (p or s) of the fundamental was controlled and that of the second harmonic independently detected to isolate specific components of the nonlinear susceptibility tensor (Fig. 1D).

If electron transfer occurs, the separation of electrons and holes across the PbSe-TiO_2 interface generates an electric field, E^{sep}, oriented in the surface normal direction (Fig. 1E). SHG is highly sensitive to such slowly varying (relative to the optical frequency) electric fields because they can perturb the symmetry of the medium (*23*). This electric-field–induced second harmonic (EFISH) response has been used to study metal-electrolyte interfaces (*24*) and buried interfaces in field-effect transistors (*25*). When an interface already exhibits a large SHG signal, $I^{2\omega}$, even without an induced interfacial field [e.g., rutile (110) under the p-in/p-out configuration in Fig. 1D], the change in the SHG intensity, $\Delta I^{2\omega}$, due to electron transfer is proportional to E^{sep} as

$$\Delta I^{2\omega} = I^{2\omega} - I_o^{2\omega} \approx \eta (I^{\omega})^2 E^{sep} \qquad (1)$$

where $I^{2\omega}$ is the intensity of the probe beam at the fundamental frequency ω, and η contains the dependence on the dielectric function through linear and nonlinear Fresnel factors as well as the wavelength-, polarization angle–, and crystallographic orientation–dependent nonlinear susceptibility [see supporting online material (SOM) text 2] (*26*). If the charge-separated PbSe-TiO_2 interface is treated as a parallel-plate capacitor, then E^{sep} and the corresponding EFISH signal scale approximately linearly with the amount of separated charge. Consequently, electron transfer dynamics may be extracted directly from the time-resolved change in SHG intensity following photoexcitation of the PbSe film.

However, the analysis is complicated by the contribution to the SHG response from the quantum dots themselves. In particular, we expect photoexcitation of the quantum dots to lead to a decrease in SHG intensity, as is observed in molecular chromophores (*16*) and semiconductor nanowires (*27*). Indeed, we measure a drop in SHG intensity upon photoexcitation of our PbSe films supported on amorphous silica glass (at all quantum dot sizes, treatments, and temperatures). Because glass has a bandgap too wide to accept electron transfer from our quantum dots, we attribute this reduced intensity to their intrinsic SHG response (figs. S7 to S9).

In contrast to this drop, we observe a substantial rise in SHG intensity after photoexcitation of the quantum dots on TiO_2 at 80 K (Fig. 2A). This response is consistent with efficient hot-electron transfer from PbSe to TiO_2 for several reasons. First, the SHG signal rises on a time scale shorter than that of the laser pulse (50 fs). Such an ultrafast response would be expected for

the strong-coupling limit of electron transfer. Also, because the electronic relaxation time between the first two excited states in similar-sized PbSe quantum dots has been measured as 540 fs at 300 K (*28*), electron transfer must be appreciably faster than this to outpace the cooling process. Second, the magnitude of the ultrafast SHG response decreases with increasing temperature (Fig. 2A). As the PbSe quantum dots are warmed to 300 K, the time constant for electron transfer should be largely unaffected in the strong-coupling limit. However, the electronic relaxation rate is known to increase exponentially (*28*). Thus, at higher temperatures, cooling of hot electrons can compete with hot-electron transfer (Fig. 2B). Because cooled electrons cannot transfer to TiO_2 in our samples, accelerated cooling leads to a decrease in SHG signal. As a negative control, we observe no electron transfer when we decrease the pump photon energy to below the threshold necessary to reach the conduction band minimum of TiO_2 (fig. S10).

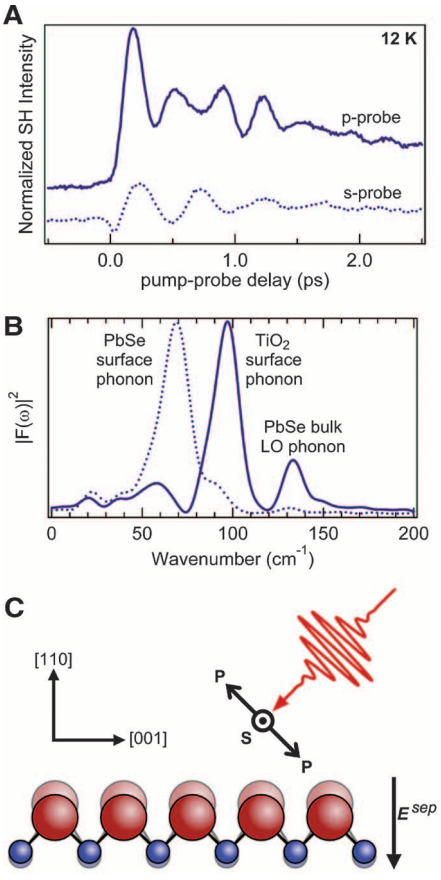

Fig. 4. Excitation of a coherent surface phonon by ultrafast electron transfer. (**A**) Time-resolved response at 12 K of the TiO_2 surface coated with 1.5 monolayers of EDT-treated 6.7-nm PbSe nanocrystals probed with either p- (solid) or s- (dotted) polarized light. (**B**) Fourier power spectrum of the oscillatory part of the SHG response curves shown in (A). With p-polarized light, a vibrational mode at 97 ± 5 cm^{-1} attributed to a rutile (110) surface-specific coherent transverse optical phonon is observed. (**C**) Coherent vibration of the Ti-O zigzag bonds running along the [001] direction of the rutile (110) surface excited by ultrafast switching-on of the interfacial electric field resulting from sub–50 fs electron transfer.

An analysis of the temperature-dependent decay of the pump-induced SHG signal on the picosecond time scale (Fig. 2C) is consistent with the temperature dependence of electron mobility in TiO_2. If an electron transfers from PbSe to a resonant energy level within the TiO_2 conduction band, this electron would have considerable kinetic energy. It would move ballistically into TiO_2, where electron-phonon scattering would bring it to the bottom of the conduction band, forming a polaron (*29*, *30*). The electric field would eventually return the electron back to the TiO_2 surface for recombination with the positively charged nanocrystal and quenching of the EFISH signal (Fig. 2C, inset). An alternative interpretation is that the injected electron diffuses deep into bulk TiO_2 and is thus screened, resulting in the decay in SHG signal. In this scenario, recombination occurs on a much longer time scale (between consecutive probe pulses). We favor the former interpretation because computational study on the single-crystal TiO_2(110) surface showed an order-of-magnitude faster time scale (~100 fs) for electron diffusion into the bulk TiO_2, whereas back electron transfer from the near-surface region of TiO_2 to electron acceptors on the surface occurs on picosecond time scales, in agreement with the SHG decay time observed here (*30*). Regardless of which mechanism is operative, the rate of decay of the interfacial electric field would be proportional to the mobility of the polaron (see SOM text 4). Previous optical measurements determined this mobility in single-crystalline rutile TiO_2 as a function of temperature (*29*). The strong correlation between the decay rate of pump-induced SHG signal enhancement and the temperature-dependent polaron mobility (Fig. 2D) supports the conclusion that we are observing hot-electron transfer to delocalized TiO_2 conduction band states.

Further evidence is provided by the influence of nanocrystal size on the SHG response at 80 K. The pump-induced SHG response has two opposite contributions: the positive response from electron transfer to TiO_2 and the negative contribution from photoexcited nanocrystals. In hydrazine-treated samples (Fig. 3A), only smaller PbSe nanocrystals (3.3 nm) exhibit a signal characteristic of efficient electron transfer. The larger quantum dots (6.1 and 6.7 nm) exhibit a sharp drop in the SHG signal at zero pump-probe delay, indicative of a dominant contribution from photoexcited nanocrystals (figs. S8 and S9). The electronic state energies in the nanocrystals are size dependent, and these observations are related to which excited states are resonant with the TiO_2 conduction band. In larger nanocrystals, this resonance occurs for highly excited electronic states (above $1P_e$) where ultrafast relaxation makes hot-electron transfer less competitive. In smaller nanocrystals, the resonance occurs for the second excited state ($1P_e$), and its relatively long lifetime makes hot-electron transfer to TiO_2 more efficient. Further, if the overall hot-electron relaxation rate could be slowed, electron transfer should compete effectively in all nanocrystal sizes. Indeed, for EDT-treated quantum dots, in which the overall electron relaxation is expected to be slower owing to effective surface passivation, we always observe the dominance of the positive SHG response from hot-electron transfer (Fig. 3B). The fluctuations in the magnitude of the pump-induced SHG signal intensity shown in Fig. 3 are representative of sample-to-sample variability in our data. We observe that these magnitude fluctuations arise primarily from batch-to-batch variations in the nanocrystals themselves and are presumably related to the structure and overall quality of the nanocrystal surface, which should play an important role in interfacial electron transfer.

One additional feature in our SHG data is the presence of large oscillations in the time-dependent response. For example, Fig. 2A shows a size-independent frequency of ~70 cm^{-1} (2.1 THz or 8.7 meV). These oscillations have larger amplitude and slower dephasing at 80 K than at 300 K and are observed with both s- and p-polarized light. Though they are not present before removal of oleic acid from the nanocrystal surface, observation of these oscillations does not require interfacial electron transfer because they occur in hydrazine- and EDT-treated PbSe films supported on SiO_2 (figs. S8 and S9). On the basis of the frequency, its invariance with quantum dot size, and the independence of substrate material, yet sensitivity to surface chemical treatment, we attribute these oscillations to a coherent surface optical phonon mode in electronically coupled two-dimensional PbSe quantum dot assemblies. Close inspection of the EDT data (Fig. 3B) reveals frequency beating in the oscillations, which becomes more apparent at lower temperatures (Fig. 4A). A frequency-domain analysis of the p-polarized SHG waveform in Fig. 4A reveals three dominant Fourier components (Fig. 4B): the previously identified PbSe surface optical mode at ~70 cm^{-1} (2.1 THz), the bulk PbSe longitudinal optical (LO) phonon at 133 ± 5 cm^{-1} (4.0 THz) (*31*), and a mode at 97 ± 5 cm^{-1} (2.9 THz) that dominates the p-polarized SHG signal but is much weaker for s-polarized probe light. The frequency of this last component is close to a predicted transverse optical phonon mode (104 cm^{-1}) of the rutile (110) surface of TiO_2, which involves the motion of Ti and O atoms in and out of the surface plane (*32*). Under the p-in/p-out configuration with our crystal orientation (Fig. 1D), the SHG response of the (110) surface originates from anharmonic polarizability of the Ti-O zigzag bonds running along the [001] direction (Fig. 4C) (*15*). As these bonds stretch and compress in phase, we observe a time-dependent modulation of the SHG intensity resulting from accompanying fluctuations of the bond hyper-

polarizability. By symmetry, this modulation should arise if the driving electromagnetic wave contains an electric-field component along the Ti-O bond. Consequently, it is only observed with a p-polarized probe beam. For the s-polarized case, the SHG response arises mainly from the PbSe quantum dots, and the coherent phonon mode at 70 cm^{-1} dominates.

We take the coherent surface phonon attributed to TiO_2 as further evidence for hot-electron transfer. Such vibrations can be excited when electric fields near the surface are activated by optical pulses shorter than the vibrational period (*33*). Electron transfer across the PbSe-TiO_2 interface within the 50-fs width of the excitation pulse establishes an interfacial electric field faster than the characteristic response time of the surface atoms. These atoms subsequently find themselves in a vibrationally excited state of the new electric-field–induced minimum energy surface configuration. Time-domain fitting of an appropriate model function to the data in Fig. 4A (see fig. S11) reveals that the initial phase of this vibration is a cosine, consistent with a displacive excitation mechanism (see SOM text 3). The phase coherence of these collective motions is then lost over time because of elastic and inelastic scattering with bulk phonons.

These results indicate that hot-electron transfer from semiconductor nanocrystals to a technologically relevant electron acceptor is possible. This effect is expected to be of general relevance to other semiconductor nanocrystals and electron and hole conductors, provided the hot electrons and holes possess sufficiently long lifetimes and the interfaces are properly controlled to enable ultrafast charge transfer. Moreover, if hot-electron (hole) transfer can be controlled to occur in very narrow energy windows to also minimize loss in the electron (hole) conductor, the highly efficient hot-carrier solar cell may be realized.

References and Notes

1. W. Shockley, H. J. Queisser, *J. Appl. Phys.* **32**, 510 (1961).
2. R. T. Ross, A. J. Nozik, *J. Appl. Phys.* **53**, 3813 (1982).
3. A. P. Alivisatos, *Science* **271**, 933 (1996).
4. A. J. Nozik, *Annu. Rev. Phys. Chem.* **52**, 193 (2001).
5. K. Mukai, M. Sugawara, in *Self-Assembled InGaAs/GaAs Quantum Dots* (Academic Press, San Diego, CA, 1999), vol. 60, pp. 209–239.
6. A. Pandey, P. Guyot-Sionnest, *Science* **322**, 929 (2008).
7. A. Pandey, P. Guyot-Sionnest, *J. Phys. Chem. Lett.* **1**, 45 (2010).
8. A. J. Nozik, *Physica E* **14**, 115 (2002).
9. N. A. Anderson, T. Q. Lian, *Annu. Rev. Phys. Chem.* **56**, 491 (2005).
10. J. L. Blackburn *et al.*, *J. Phys. Chem. B* **109**, 2625 (2005).
11. I. Robel, V. Subramanian, M. Kuno, P. V. Kamat, *J. Am. Chem. Soc.* **128**, 2385 (2006).
12. B. R. Hyun *et al.*, *ACS Nano* **2**, 2206 (2008).
13. S. Y. Jin, T. Q. Lian, *Nano Lett.* **9**, 2448 (2009).
14. Y. R. Shen, *Nature* **337**, 519 (1989).
15. M. Omote *et al.*, *J. Phys. Cond. Mat.* **17**, S175 (2005).
16. E. A. McArthur, K. B. Eisenthal, *J. Am. Chem. Soc.* **128**, 1068 (2006).
17. D. V. Talapin, C. B. Murray, *Science* **310**, 86 (2005).
18. F. W. Wise, *Acc. Chem. Res.* **33**, 773 (2000).
19. See supporting material on *Science* Online.
20. D. Yu, C. J. Wang, P. Guyot-Sionnest, *Science* **300**, 1277 (2003).
21. J. M. Luther *et al.*, *ACS Nano* **2**, 271 (2008).
22. K. J. Williams *et al.*, *ACS Nano* **3**, 1532 (2009).
23. T. F. Heinz, in *Nonlinear Surface Electromagnetic Phenomena*, H. Ponrath, G. Stegeman, Eds. (Elsevier, Amsterdam, 1991), pp. 353–416.
24. R. M. Corn, D. A. Higgins, *Chem. Rev.* **94**, 107 (1994).
25. O. A. Aktsipetrov *et al.*, *Phys. Rev. B* **60**, 8924 (1999).
26. A. Nahata, T. F. Heinz, *Opt. Lett.* **23**, 67 (1998).
27. J. C. Johnson *et al.*, *Nano Lett.* **4**, 197 (2004).
28. R. D. Schaller *et al.*, *Phys. Rev. Lett.* **95**, 196401 (2005).
29. E. Hendry, F. Wang, J. Shan, T. F. Heinz, M. Bonn, *Phys. Rev. B* **69**, 081101 (2004).
30. O. V. Prezhdo, W. R. Duncan, V. V. Prezhdo, *Prog. Surf. Sci.* **84**, 30 (2009).
31. R. N. Hall, J. H. Racette, *J. Appl. Phys.* **32**, 2078 (1961).
32. R. Lindsay *et al.*, *Phys. Rev. Lett.* **94**, 246102 (2005).
33. Y. M. Chang, L. Xu, H. W. K. Tom, *Phys. Rev. Lett.* **78**, 4649 (1997).

34. We thank K. S. Leschkies, A. Wolcott, C. Nelson, and G. Haugstad for assistance with PbSe nanocrystal synthesis and atomic force microscopy imaging. This work was supported by the U.S. Department of Energy (DE-FG02-07ER46468). Partial support from the NSF Nanoscale Interdisciplinary Research Team (NIRT) program (CBET-0506672) and the Materials Research Science and Engineering Center (MRSEC) programs (DMR-0819885) in the form of student assistantships to B.A.T. and W.A.T. are acknowledged. W.A.T. received support from a University of Minnesota Doctoral Dissertation Fellowship.

Supporting Online Material

www.sciencemag.org/cgi/content/full/328/5985/1543/DC1
Materials and Methods
SOM Text
Figs. S1 to S11
Table S1
References

3 December 2009; accepted 4 May 2010
10.1126/science.1185509

Crossover from Single-Step Tunneling to Multistep Hopping for Molecular Triplet Energy Transfer

Josh Vura-Weis,[1] Sameh H. Abdelwahed,[2] Ruchi Shukla,[2] Rajendra Rathore,[2]* Mark A. Ratner,[1]* Michael R. Wasielewski[1]*

Triplet energy transfer (TT), a key process in molecular and organic electronics, generally occurs by either strongly distance-dependent single-step tunneling or weakly distance-dependent multistep hopping. We have synthesized a series of π-stacked molecules consisting of a benzophenone donor, one to three fluorene bridges, and a naphthalene acceptor, and studied the rate of TT from benzophenone to naphthalene across the fluorene bridge using femtosecond transient absorption spectroscopy. We show that the dominant TT mechanism switches from tunneling to wire-like hopping between bridge lengths 1 and 2. The crossover observed for TT can be determined by direct observation of the bridge-occupied state.

The rapid and efficient transport of energy and charge over tens to hundreds of nanometers in molecules underlies the performance of devices such as organic photovoltaics, thin-film transistors, and light-emitting diodes. Charge and energy transport is also crucial to many biological processes, such as long-distance electron transfer in proteins (*1*) and the quenching of triplets in the bacterial photosynthetic reaction center by energy transfer cascades. (*2*) The study of charge transfer (CT) and triplet energy transfer (TT) in donor-bridge-acceptor (D-B-A) systems has demonstrated two general transport mechanisms—strongly distance-dependent single-step tunneling and weakly distance-dependent multistep hopping, which is also known as wire-like transport (*3*). Optimizing TT efficiency is particularly important for improving organic and polymer light-emitting diode (OLED/PLED) performance, because injection of charge into the active layer of these devices generally leads to a 3:1 ratio of triplet to singlet excitons through spin statistics (*4*, *5*), although the singlet exciton population may be higher in π-conjugated polymers (*6*). TT in PLEDs occurs both within and between chains (*7*), so that transport through noncovalent π-stacked molecules is important.

A major goal is to design molecules that exhibit multistep hopping in which charge or energy moves from a donor to the bridge and then later to the acceptor. Several CT studies have shown a crossover from tunneling to hopping as the bridge length increased, which

[1]Department of Chemistry and Argonne-Northwestern Solar Energy Research (ANSER) Center, Northwestern University, Evanston, IL 60208, USA. [2]Department of Chemistry, Marquette University, Post Office Box 1881, Milwaukee, WI 53201, USA.

*To whom correspondence should be addressed: rajendra.rathore@marquette.edu (R.R.); ratner@chem.northwestern.edu (M.A.R.); m-wasielewski@northwestern.edu (M.R.W.)